ELSEVIER

Coordination Chemistry Reviews 233–234 (2002) 63–73

COORDINATION CHEMISTRY REVIEWS

www.elsevier.com/locate/ccr

Coupling between normal coordinates in the ground and excited states of coordination compounds. Electronic spectroscopy and theoretical models

Julie Landry-Hum, Véronique Tessier, Matthias Ernzerhof, Christian Reber *

Département de chimie, Université de Montréal, C.P. 6128, Succ. Centre-ville, Montréal, QC, Canada H3C 3J7

Received 27 November 2001; accepted 8 March 2002

Contents

Abstract

Effects of coupling between normal coordinates can be analyzed from absorption and emission spectra. The spectroscopic phenomena reviewed here arise from interactions between electronic states with different equilibrium structures, a situation that leads to coupled coordinates. They have received some attention in the past for special categories of coordination compounds, such as Jahn-Teller active high-symmetry transition metal complexes and mixed valence compounds. We use model systems outside these established categories and illustrate the spectroscopic effects with calculations involving two normal coordinates and two electronic states. These models show directly how coordinate coupling arises as a consequence of the non-crossing rule for states of identical symmetry and they are easily generalized to other molecular systems with energetically close electronic states. Electronic structure calculations are presented to further illustrate the effects of coupling. The examples analyzed are based on experimental results reported for *trans*-dioxo complexes of rhenium(V) and chromium(III) fluorides.

Keywords: Absorption spectroscopy; Luminescence spectroscopy; Vibronic structure; Time-dependent theory of spectroscopy; Potential energy surfaces

1. Introduction

Traditionally, molecular electronic states are described by a single potential energy surface defined along the normal coordinates of the molecule. In this approximation, electronic transitions in absorption or luminescence spectra involve two potential energy surfaces, corresponding to the initial and final states of the transition. Interactions with other states are neglected or assumed to simply lead to changes of the overall intensity of bands in electronic spectra. An example is the intensity increase of a weak band corresponding to a forbidden transition in an absorption spectrum through coupling with a nearby allowed transition [1]. Other spectroscopic manifestations of interactions between states on vibronic bandshapes have received less attention. A few situations have been analyzed with coupled potential energy curves defined along a single normal coordinate. These one-

* Corresponding author. Tel.: +1-514-343-7332; fax: +1-514-343-7586.
E-mail address: reber@chimie.umontreal.ca (C. Reber).

0010-8545/02/$ - see front matter
PII: S0010-8545(02)00096-6

dimensional models can be used to characterize some effects of coupling between electronic states, but obviously no coupling between normal coordinates can be examined with this approach [1,2]. The validity and limitations of one-dimensional models have been explored in detail for several compounds using single-crystal absorption and luminescence spectroscopy at low temperature or under high external pressure [1–8]. The goal of this overview is to examine interacting states defined along two normal coordinates in order to illustrate aspects of vibronic spectra beyond the one-dimensional models. The interaction between these electronic states leads to an intrinsic coupling between normal coordinates. In addition, we present results of electronic structure calculations that also indicate the presence of coupling between normal coordinates.

A significant number of recent publications, mainly using advanced computational tools, have led to new insight on coupled coordinates [9–12]. Dynamic studies aimed at small polyatomic molecules and photochemical product distributions [13,14] have been reported, and a few analyses of coupled coordinates through spectroscopy and theoretical calculations of spectra have been published [15–17]. The vast majority of these studies investigate molecules that are not coordination compounds, a somewhat surprising fact, as transition metal complexes with their rich electronic structure and significant spin–orbit coupling between states are highly susceptible to effects arising from interacting electronic states. Exceptions to this situation are Jahn-Teller systems [18] and intervalence compounds [17,19]; both recently reviewed in depth.

Coupling between normal coordinates can arise as a consequence of interacting electronic states. We illustrate such effects with the simplest possible model: two electronic states described by potential energy surfaces along two normal coordinates. Effects such as spin–orbit coupling and configuration interaction can lead to distinct bandshapes and vibronic structure in the absorption and luminescence spectra of many coordination compounds and organometallic molecules. We present calculations for two specific situations, illustrated schematically with the one-dimensional cross sections along a single normal coordinate Q_i in Fig. 1. All parameters defining the models in Fig. 1 are given in Section 2. The first situation of interest involves the electronic ground state interacting with an excited electronic state, as shown in Fig. 1a. The coupling between the states leads to a ground state potential energy surface that is flattened in the region below the minimum of the excited state potential surface. The bandshape and vibronic structure in the luminescence spectrum are affected by this coupling. The model in Fig. 1a is inspired by the experimental spectra of *trans*-dioxo complexes of rhenium(V) and osmium(VI) [20–25]. Instead of carrying out the calculation of a spectrum

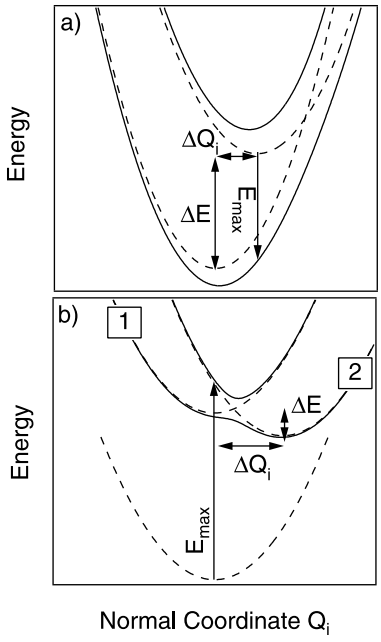

Fig. 1. (a) Coupled one-dimensional potentials along a single normal coordinate Q_i illustrating the luminescence transition analyzed in Section 2. (b) Coupled excited-state potentials along a single normal coordinate Q_i, illustrating the absorption transition analyzed in Section 3. Adiabatic and diabatic (harmonic) potentials are shown as solid and dotted lines, respectively. The labels 1 and 2 denote the diabatic potentials of the final states for the absorption transition analyzed in Section 3.

with the full ensemble of diabatic and adiabatic potential energy surfaces, it is sufficient in this case to include only the adiabatic ground state potential surface, corresponding to the lower solid curve in Fig. 1a, as the final state of the transition in the calculation of a spectrum. The mixing between the states is small and the crossing between their potential energy surfaces occurs far from the Franck–Condon region of the luminescence transition, shown as a vertical arrow in Fig. 1a. Nevertheless, the coupling between states has to be considered, because it significantly alters the shape of the ground state potential energy surface, as illustrated by the difference between the adiabatic (solid line) and diabatic (harmonic, dotted line) ground state potentials in Fig. 1a. Detailed density functional calculations are used as an alternative approach to characterize a *trans*-dioxo rhenium(V) complex, qualitatively confirming the presence of coupled normal coordinates. This example illustrates the importance of coupling along normal coordinates on the ground state potential energy surface arising through interactions with an energetically well-separated excited state, an effect that is usually neglected in studies of transition metal compounds.

More dramatic effects of coupled coordinates are observed for interacting electronic states that are close in energy. This situation typically occurs for excited states of transition metal compounds and can be analyzed

from absorption spectroscopy, as schematically illustrated in Fig. 1b. Strong mixing occurs between such states and the full set of diabatic and adiabatic potential energy surfaces has to be used for an adequate description of the final state of the electronic absorption transition, shown as a vertical arrow in Fig. 1b. The crossing of the diabatic potential energy surfaces occurs near the Franck–Condon transition, and the two coupled excited states have an important influence on the absorption spectrum [2]. In the literature, the overlapping lowest spin-allowed and -forbidden transitions in chromium(III) and vanadium(II) complexes with the d^3 electron configuration are the most common examples of absorption spectra showing effects of coupling between states and coordinates [2,26–32]. Such effects are expected to occur for many other compounds if states arising from different electron configurations are close in energy, as illustrated schematically for the excited states labeled 1 and 2 in Fig. 1b. These labels were chosen to be coherent with an earlier review on spectroscopic effects arising from coupled one-dimensional potential curves [1]; for a transition metal complex with the d^3 electron configuration they correspond to the lowest doublet and quartet excited states, respectively. The transition from the quartet ground state to the doublet excited state is assumed to borrow its intensity entirely from the allowed transition to the quartet excited state.

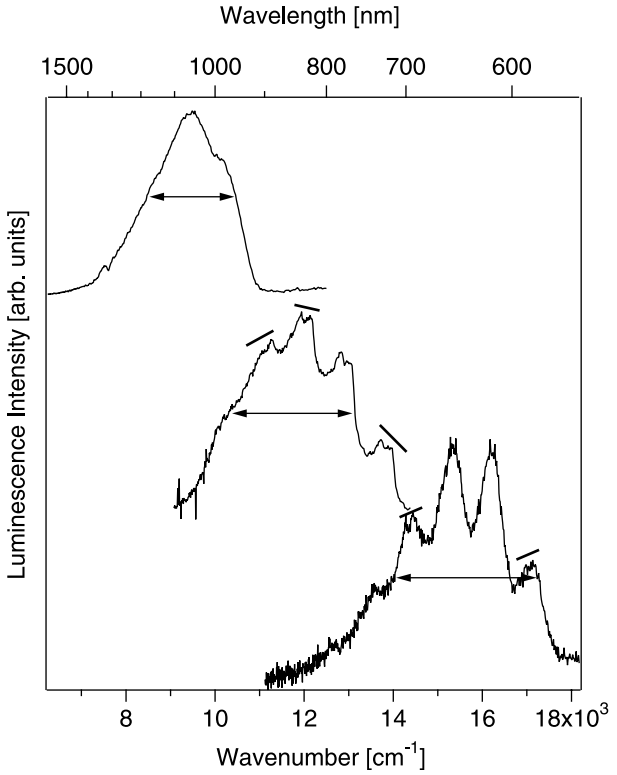

Fig. 2. Experimental low-temperature single-crystal luminescence spectra of rhenium(V)-oxo complexes. Top to bottom: ReO(diphenylphosphino)phenolate)$_2$Cl (10 K), *trans*-ReO$_2$(ethylenediamine)$_2$Cl (15 K), *trans*-ReO$_2$(*N*,*N*,*N*′,*N*′-tetramethylethylenediamine)$_2$Cl (10 K).

Even in the absence of well resolved vibronic structure in an experimental spectrum, features such as interference dips [2] can be observed and allow us to analyze the coupling between electronic states and normal coordinates. The interference dip in molecular absorption spectra has often been denoted as a Fano antiresonance [28]. An exact quantitative relationship illustrating the crucial differences between Fano's approach for atomic transitions and molecular spectra has only recently been published [33]. Our calculations show that the shape of the interference dip in absorption spectra reflects the influence of coupled coordinates [26], an effect that can be observed even in absorption spectra without resolved vibronic structure.

The spectroscopic effects arising from the situations illustrated in Fig. 1 with two normal coordinates Q_i (i = 1, 2) are distinctly different from those that can be obtained with one-dimensional models involving only a single coordinate [1]. These effects are most easily seen in cases where the vibrational frequencies of the two modes are significantly different, as this leads to well-separated vibronic transitions that can be distinguished in experimental spectra.

2. Coupling between coordinates in the electronic ground state. Band envelopes and vibronic structure in luminescence spectra

This section is inspired by the detailed vibronic structure observed for *trans*-dioxo complexes of rhenium(V), such as *trans*-ReO$_2$(ethylenediamine)$_2^+$ [20–25]. The vertical energy difference between the ground and lowest-energy excited state in these compounds is on the order of 9000–20 000 cm^{-1}. The detailed analysis of the spectra shows that coupling effects can be observed despite the considerable energy separations between electronic states, especially for third row transition metal complexes with their large spin–orbit coupling constants. Rhenium-oxo complexes are particularly appropriate for such a study because they have metal–ligand stretching modes with very different frequencies and the high-frequency metal–oxo mode has been shown to have a normal coordinate involving almost exclusively the O=metal=O fragment [34].

Fig. 2 illustrates low-temperature single-crystal luminescence spectra of three rhenium(V)-oxo complexes [24,25]. All spectra show a main vibronic progression involving the symmetric rhenium–oxo stretching mode with a frequency of ca. 900 cm^{-1}. Two important trends are observed. First, the band width decreases as the energy of the band maximum E_{max} and the separation ΔE between the electronic states in Fig. 1a decrease, as illustrated by the horizontal double arrows in Fig. 2.

Second, the vibronic structure shows an unusual variation: for large values of E_{max} and ΔE, the intensity distribution within each peak of the high-frequency progression does not vary, as indicated by the lines with identical slopes added to the first and fourth member of the main progression in the bottom spectrum of Fig. 2. The middle spectrum in Fig. 2 corresponds to lower values of E_{max} and ΔE and shows a distinct variation of the intensity distribution along the main progression, as indicated by the lines with different slopes given above the first, third and fourth members of the main progression. Such non-replica patterns are a characteristic signature of coupled coordinates. The lowest energy spectrum, shown as the top trace in Fig. 2, is expected to show the most distinct non-replica pattern, but it is not sufficiently resolved to observe this effect. The model defined in the following rationalizes the two trends illustrated by the experimental spectra in Fig. 2.

In order to explore the luminescence spectroscopy of the rhenium-oxo complexes and other compounds with coupled coordinates in the electronic ground state, we define the interacting states using potential energy surfaces. Fig. 1a shows a one-dimensional schematic view, illustrating the coupling between the ground and emitting states. Of interest here are situations with offsets of the potential minima along two coordinates. The potential energy V of the coupled states along the normal coordinates Q_1 and Q_2 in dimensionless units is given by:

$$V = \begin{pmatrix} 1/2(k_1Q_1^2 + k_2Q_2^2) & V_{12} \\ V_{12} & 1/2(k_1(Q_1 - \Delta Q_1)^2 + k_2(Q_2 - \Delta Q_2)^2) + \Delta E \end{pmatrix} \quad (1)$$

The diagonal elements of Eq. (1) correspond to the diabatic potentials, chosen to be harmonic for this overview and given as dotted lines in Fig. 1. k_1 and k_2 denote the vibrational frequencies of the two normal modes in wavenumber units. They are assumed to be identical for the ground and excited states throughout the following. The offsets between potential minima along Q_1 and Q_2 are denoted by ΔQ_1 and ΔQ_2, respectively. The diabatic potential minima are separated by ΔE. These quantities are illustrated schematically in Fig. 1. The coupling between states is given by the constant V_{12}.

The eigenvalues of Eq. (1) correspond to the adiabatic potential energy surfaces illustrated by the solid lines in Fig. 1. For Eq. (1), the eigenvalues $E_{a1,a2}$ can be calculated analytically as:

$$E_{a1,a2} = \frac{1}{4}(2k_1Q_1^2 + 2k_2Q_2^2 - 2\Delta Q_1k_1Q_1 - 2\Delta Q_2k_2Q_2$$

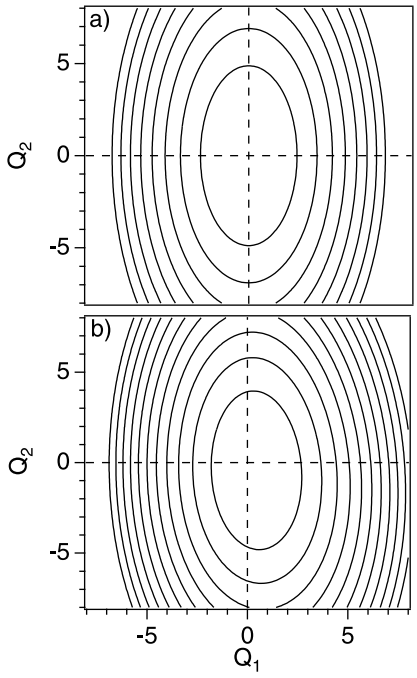

Fig. 3. (a) Harmonic potential energy surface as a function of two normal coordinates in dimensionless units. (b) Two-dimensional adiabatic ground state potential energy surface used to calculate the spectra in Fig. 4b. All parameters used to define these surfaces are given in Table 1.

$$+2\Delta E + k_1\Delta Q_1^2 + k_2\Delta Q_2^2$$

$$\pm[8\Delta Q_1\Delta Q_2k_1k_2Q_1Q_2 + 4k_1^2\Delta Q_1^2Q_1^2 + 4k_2^2\Delta Q_2^2Q_2^2$$

$$-(4k_1^2\Delta Q_1^3 + 8k_1\Delta Q_1\Delta E + 4k_1k_2\Delta Q_1\Delta Q_2^2)Q_1$$

$$-(4k_2^2\Delta Q_2^3 + 8k_2\Delta Q_2\Delta E + 4k_1k_2\Delta Q_2\Delta Q_1^2)Q_2 + 4\Delta E^2$$

$$+ 4\Delta E(k_1\Delta Q_1^2 + k_2\Delta Q_2^2)$$

$$+2\Delta Q_1^2\Delta Q_2^2k_1k_2 + k_1^2\Delta Q_1^4 + k_2^2\Delta Q_2^4 + 16V_{12}^2]^{1/2}) \quad (2)$$

This result allows us to identify the coupling term between coordinates. Only expressions depending on both Q_1 and Q_2 can lead to coupling. The only such term in Eq. (2) is the first addend in the sum under the square root, $8k_1k_2\Delta Q_1\Delta Q_2Q_1Q_2$, all other terms are either constants, leading to a simple shift of the spectrum along the energy axis, or they involve only one of the two coordinates and can therefore not contribute to coupling. The analytical coupling term shows that only normal coordinates with non-zero offsets ΔQ_i can be coupled, an aspect that severely limits the number of coordinates that have to be included in a model.

The simplest coupling term reported in the literature is the product Q_1Q_2, leading to the Duschinsky effect [35]. Other terms proposed and applied are of the form $Q_1Q_2^2$ [16,36]. All these terms have to be combined with an adjustable factor in order to lead to calculated spectra in good agreement with experiment. The magnitude of this factor is usually a phenomenological fit parameter [16,22]. In contrast, the coupling term given in Eq. (2) involves only quantities that can be determined or at least estimated from spectroscopic experiments.

Fig. 3 shows the ground state potential energy surface corresponding to the final state in Fig. 1a as a contour plot involving both Q_1 and Q_2. The diabatic surface is given in Fig. 3a. The minimum of this contour plot is at the origin of the Q_1, Q_2 coordinate system (dotted lines), as expected from the upper diagonal element in Eq. (1). The lower-energy eigenvalue in Eq. (2) is shown in Fig. 3b. All parameters used to calculate the contour plots in Fig. 3 are given in Table 1. Two important manifestations of coupling are obvious from the comparison of the contour plots in Fig. 3. First, the ground state minimum is shifted along Q_1 and Q_2 toward the minimum of the excited state. This effect can also be seen in the one-dimensional schematic view shown in Fig. 1a. The second important difference between the contour plots is the counterclockwise 'tilt' of the adiabatic potential energy surface in Fig. 3b, easily seen from the innermost contour line and the right hand edge of the figure. This effect cannot be seen in the one-dimensional representation in Fig. 1a and is a characteristic aspect of coupling between normal coordinates.

Luminescence spectra arising from the final state potential in Fig. 3b are calculated using numerical grids of 256^2 points to represent potentials and wavefunctions. The approach using time-dependent theory [37,38] has been described in detail before [1,39–41] and a detailed

Table 1
Parameters defining the coupled potentials along two normal coordinates in Eqs. (1) and (2). The potentials are used to calculate the luminescence and absorption spectra shown in Figs. 4 and 9

Parameter	Luminescence calculation	Absorption calculation
k_1 (cm^{-1})	880	600
k_2 (cm^{-1})	210	230
ΔQ_1	2.66	2.76
ΔQ_2	−1.50	2.62
V_{12} (cm^{-1})	5000	700
ΔE (cm^{-1})	3000	−8000
	7000	−6000
	11 000	−4000
	13 000	−2000
		0
		2000

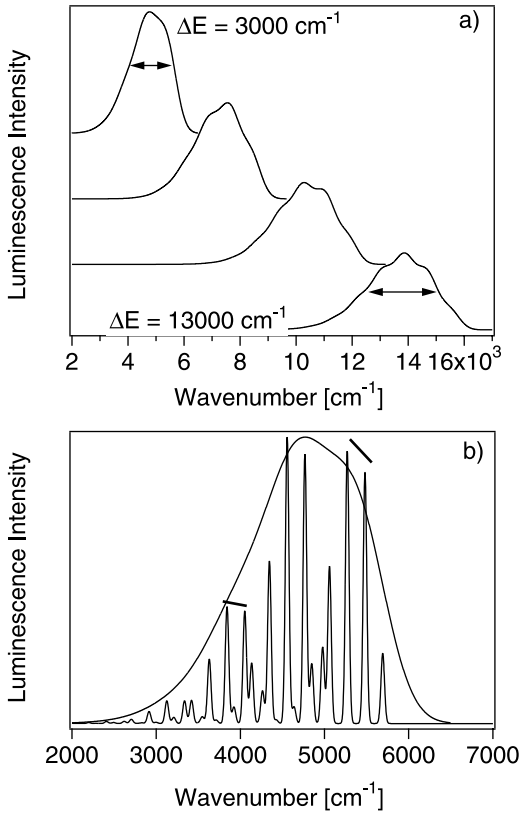

Fig. 4. (a) Calculated low-resolution luminescence spectra from the two-dimensional potentials defined in Table 1. Spectra are offset along the ordinate for clarity and ΔE increases from top to bottom through the list of values given in Table 1. (b) Low and high resolution calculated spectra for $\Delta E = 3000\ cm^{-1}$, corresponding to the top trace in (a).

view of the time evolution of a wavefunction on potentials similar to those in Fig. 3 has been published [42]. Fig. 4 shows calculated luminescence spectra using the parameters in Table 1 for several values of ΔE. The band envelopes in Fig. 4a clearly illustrate the influence of coupling between electronic states. The lowest trace, corresponding to the largest separation ΔE between the states, shows a bandshape very close to the one expected for transitions between harmonic potentials with minima displaced along the normal coordinates Q_1 and Q_2 by ΔQ_1 and ΔQ_2, respectively. As ΔE decreases, the bandshape becomes narrower, despite the constant values of ΔQ_1 and ΔQ_2. This effect is caused by the coupling between electronic states, leading to a flattening of the ground state potential illustrated in Fig. 1a and Fig. 3b that becomes more important for states that are close in energy. The decrease in the overall bandwidth is easily identified from the experimental luminescence spectra in Fig. 2.

Fig. 4b shows the calculated spectrum for the lowest value of ΔE, corresponding to the top trace in Fig. 4a, at both low and high resolution. Highly resolved spectra allow a direct observation of the effects of coupling

between modes. The vibronic structure consists of clusters of peaks separated by the vibrational energy of the high-frequency mode [16]. Each cluster is formed by vibronic transitions separated by the low vibrational frequency. The distribution of relative intensities within each cluster is identical in the absence of coupling between normal coordinates [36], leading to a replica pattern as shown by the lines with identical slopes in the bottom spectrum of Fig. 2. In contrast, the calculated resolved spectrum in Fig. 4b clearly shows a non-replica pattern, illustrated by the sloping lines on the high and low energy sides of the luminescence spectrum, qualitatively similar to the variation observed in the middle spectrum of Fig. 2. This distinct variation of vibronic intensities indicates coupling between coordinates. It can be reproduced by a variety of simple coupling terms, such as the examples given above. In general, the information of a single experimental spectrum is not sufficient to distinguish between different choices of coupling terms. The comparison of spectra from a series of related molecules, as illustrated in Fig. 2, is essential to establish trends as shown in Fig. 4, which point towards interacting states as the physical origin of coupling between coordinates. The effects of coupling on the calculated spectra in Fig. 4 are not very strong. It has been shown for *trans*-dioxo complexes of rhenium(V) that coupling between the ground state and only a single excited state is not sufficient to quantitatively reproduce the observed non-replica pattern in resolved spectra, but that both spin–orbit coupling and configuration interaction to several excited states have to be considered [24]. The model defined by Eqs. (1) and (2) can easily be generalized to include multiple excited states, but the terms coupling the coordinates are then no longer as simple as the single coupling term in Eq. (2).

An alternative to the model based on the simple potential energy surfaces defined in Eq. (1) are electronic structure calculations. We use advanced DFT methods and perform calculations for *trans*-ReO_2(ethylenediamine)$_2^+$, a well studied representative *trans*-dioxo complex of rhenium(V), whose luminescence spectrum is shown as the middle trace in Fig. 2. The calculations are performed with the development version of GAUSSIAN-99 [43] using the LanL2DZ pseudopotential and basis set combination. In the Kohn–Sham calculation we employ the PBE hybrid approximation [44–46] to the exchange-correlation energy. For the calculation of frequencies the LSD functional (USVWN5 keyword in GAUSSIAN) is used as well for comparison. The calculated structure for the complex is in good agreement with the experimental crystal structure [47]. Re=O bond lengths of 1.774 Å are calculated, deviating by about 0.5% from the crystallographic bond lengths of 1.765 Å [47] and illustrating the high quality of our calculations, particularly in comparison to a recent comprehensive computational investigation of oxo and nitrido complexes of a series of second and third row transition metal ions [48]. The compound in the literature study most similar to our target is $ReOCl_4$, containing a rhenium(VI) center with a calculated metal–oxo bond length of 1.611 Å, longer by 3% than the crystallographic value [48]. We calculate Re–N(ethylenediamine) bond lengths of 2.173 Å, again in very good agreement with the average crystallographic value of 2.152 Å for the four bonds [47]. It is interesting to note that the calculations for *trans*-ReO_2–(N,N,N',N'-tetramethylethylenediamine)$_2^+$, whose luminescence spectrum is shown as the bottom trace of Fig. 2, lead to the same Re=O bond lengths as for *trans*-ReO_2(ethylenediamine)$_2^+$, but the Re–N bond lengths in the former complex are calculated to be 2.241 Å, longer by 3% than in the calculation for the latter compound. This increase in bond length possibly contributes to the higher energy luminescence band maximum for *trans*-ReO_2(N,N,N',N'-tetramethyl–*ethylenediamine*)$_2^+$ illustrated in Fig. 2 and discussed in an earlier overview [23]. The HOMO, LUMO and LUMO+1 orbitals correspond to the expected d_{xy}, d_{xz}, d_{yz} triad [49], with the z axis chosen parallel to the Re=O bonds. The different metal–ligand electron densities of the $(d_{xy})^2$ and $(d_{xy})^1(d_{xz,yz})^1$ configurations lead to large ΔQ_i values along the normal coordinates involving the Re=O and Re–N bonds, justifying their importance for the analysis of coupled coordinates based on the coupling term in Eq. (2).

Symmetric O=Re=O stretching frequencies of 926 and 953 cm^{-1} are calculated for the *trans*-ReO_2(ethylenediamine)$_2^+$ complex with the LSD and PBE hybrid methods, respectively. These values are higher by 5 and 8% than the experimental frequency of 880 cm^{-1} [21,23,24], but again in better agreement with the experiment than reported in the literature for $ReOCl_4$ [48], where a value of 1229 cm^{-1} is calculated, higher by 18% than the experimental frequency of 1040 cm^{-1}. For the Re–ethylenediamine stretching mode, frequencies of 233 and 235 cm^{-1} are obtained from the LSD and PBE hybrid methods, respectively, in very good agreement with the experimental value of 210 cm^{-1} [21,23,24]. The calculated potential energy at a series of discrete values along the O=Re=O coordinate Q_1 is denoted by the dots in Fig. 5a and compared to the harmonic potential curve obtained with the calculated frequency of 953 cm^{-1}, shown as a solid line in Fig. 5a. Near the ground-state equilibrium geometry, the harmonic potential closely resembles the numerical potential curve, indicating that the discrepancy between the calculated harmonic frequency and the experimental value is not due to the harmonic approximation. The DFT results show that the potential is flattened at high values of Q_1, in qualitative agreement with the experimental findings and the adiabatic potential shown in

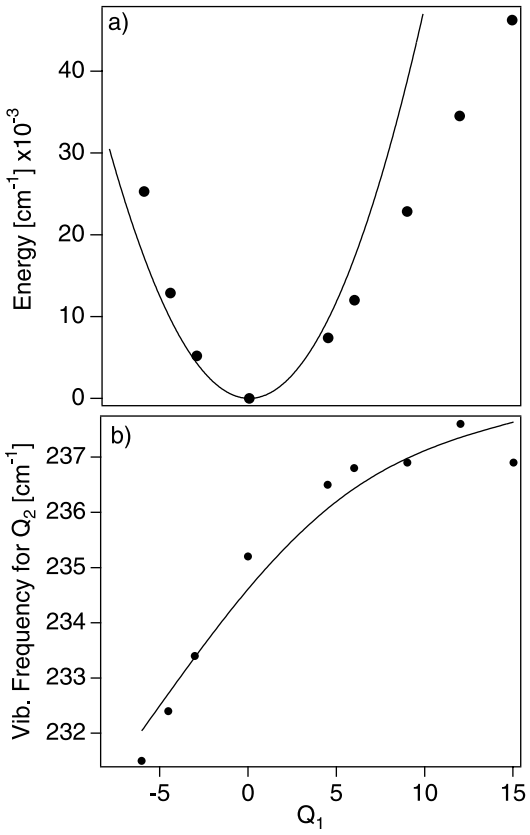

Fig. 5. (a) Calculated potential energy curve for *trans*-ReO_2(ethylenediamine)$_2^+$ along the O=Re=O symmetric stretching coordinate obtained from DFT (dots) and from the harmonic approximation using a frequency of 953 cm^{-1} (solid line). (b) Re–(ethylenediamine) symmetric stretching frequency calculated for each value of the normal coordinate in (a). The solid line is a guide for the eye.

Fig. 3b. Currently, we are not able to include spin–orbit coupling into the DFT calculation and this is probably the explanation for the discrepancy between the calculated and experimental value of the symmetric O=Re=O stretching frequency. Consequently, we did not attempt to calculate a full two-dimensional potential energy surface. In order to probe for coupled coordinates, we have calculated the totally symmetric Re–(ethylenediamine) stretching frequency for a series of discrete values of the normal coordinate Q_1. For uncoupled coordinates, this vibrational frequency is expected to be constant. Fig. 5b shows that the frequency varies significantly along Q_1, demonstrating that DFT calculations can be used to qualitatively indicate the presence of coupling between coordinates.

3. Coupling between coordinates in excited states. Interference dips in absorption spectra

Excited states that are close in energy can give rise to easily discernible spectroscopic manifestations of coupling. The example discussed in the following involves

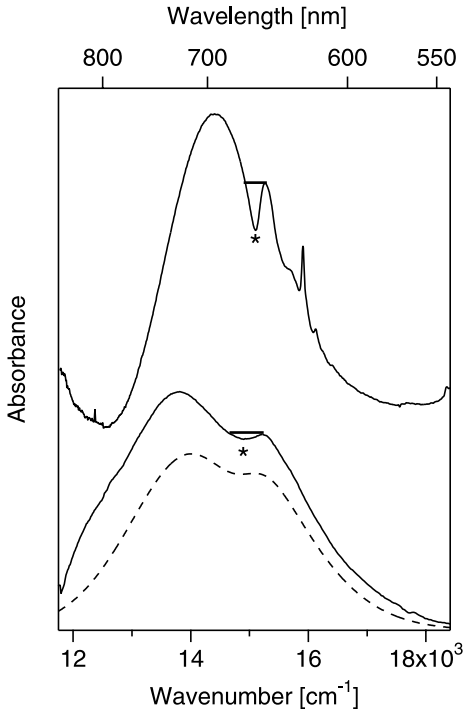

Fig. 6. Absorption spectra showing interference dips denoted by asterisks. Solid and dotted traces denote experimental and calculated spectra, respectively. Top trace: single crystal absorption spectrum of $Cr_2F_9^{3-}$ measured at 15 K. Middle trace: room temperature absorption spectrum of $Ni(H_2O)_6^{2+}$ in solution. Bottom trace: calculated spectrum of $Ni(H_2O)_6^{2+}$ with one-dimensional potential energy curves.

interference dips [2] in absorption spectra, arising from the situation schematically illustrated in Fig. 1b. In contrast to Section 2, the limitation to a single adiabatic surface is no longer an acceptable approximation. We need the full set of potentials defined by the matrix in Eq. (1) and have to include wavefunction amplitude transfer between the coupled states [1,2,4,5]. Again, the potentials defined by Eq. (1) and time-dependent theory lead to calculated spectra and an intuitive understanding of spectroscopic effects.

Fig. 6 illustrates interference dips in two absorption spectra. We compare the single-crystal absorption spectrum of $Cr_2F_9^{3-}$ [26], polarized perpendicular to the trigonal axis of the chromophore, and the solution absorption spectrum of $Ni(H_2O)_6^{2+}$ [5,50]. Asterisks indicate the interference dips, which occur at similar energies in the two compounds and correspond to band systems involving two coupled excited states, as illustrated in Fig. 1b. The horizontal lines above the interference dips indicate their widths of 340 and 680 cm^{-1} for $Cr_2F_9^{3-}$ and $Ni(H_2O)_6^{2+}$, respectively. The single-crystal spectrum of $Cr_2F_9^{3-}$ shows additional weak bands superimposed on the high-energy side of the broad band. They correspond to spin-forbidden transitions to doublet excited states that interact only very weakly or not at all with the allowed transition and are outside the scope of our model. The spectrum of

$Ni(H_2O)_6^{2+}$ illustrates that low temperature is not always required to observe vibronic effects caused by coupled excited states. This experimental spectrum has been analyzed in detail and it compares very favorably to the calculated spectrum, shown as a dotted line in Fig. 6. This calculation is based on one-dimensional potential curves as illustrated in Fig. 1b, using the vibrational energy of the symmetric nickel–water stretching mode with a frequency of 355 cm^{-1} [5,50]. Similar calculations based on one-dimensional potential energy curves also rationalize the additional vibronic structure resolved in the low-temperature single crystal spectra of this and related complexes [5]. The width of the interference dip is 680 cm^{-1}, approximately twice the nickel–water vibrational frequency. This relationship applies to all spectra calculated from one-dimensional potential curves, and it immediately reveals that the much narrower width of the interference dip in the spectrum of $Cr_2F_9^{3-}$ is smaller by a factor of two than expected from a one-dimensional model based on the frequencies of 400–500 cm^{-1} measured for the chromium–fluoride stretching modes [26]. In the following, we show how coupled coordinates can affect interference dips in absorption spectra.

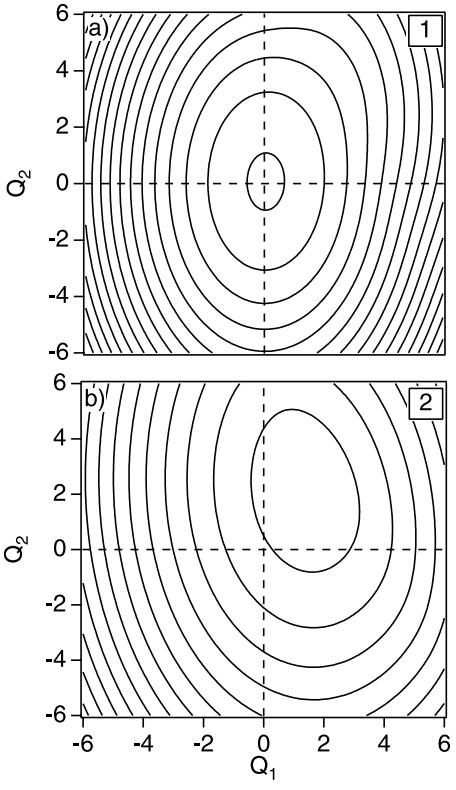

Fig. 7. Two-dimensional adiabatic potentials illustrating the effects of coupling beween states and coordinates. The energy difference ΔE between the minima of states 1 and 2 is 2000 cm^{-1}. For octahedral chromium(III) complexes, states 1 and 2 correspond to the lowest energy doublet and quartet excited states, respectively, with the potential energy minimum of the doublet surface lower than the minimum of the quartet surface.

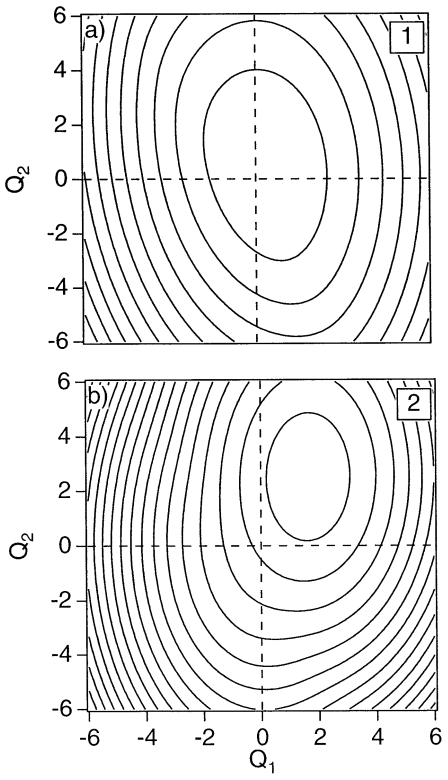

Fig. 8. Two-dimensional adiabatic potentials illustrating the effects of coupling beween states and coordinates. The energy difference ΔE between the minima of states 1 and 2 is -2000 cm^{-1}. For octahedral chromium(III) complexes, states 1 and 2 correspond to the lowest energy doublet and quartet excited states, respectively, with the potential energy minimum of the quartet surface lower than the minimum of the doublet surface.

Interference dips have been observed most often for octahedral complexes of chromium(III). The electronic ground state of these compounds is $^4A_2$ and coupling is observed between the ^2E and $^4T_2$ excited states. The model used here is simplified and includes only a single doublet (^2E) and a single quartet ($^4T_2$) potential energy surface, denoted as states 1 and 2 in Figs. 1b, 7 and 8. The energy differences ΔE discussed in the following are obtained by subtracting the energy of the potential surface minimum of state 1 from the minimum energy of state 2. The doublet excited state corresponds to state 1 and its diabatic potential energy minimum is directly above the ground state minimum, as the two states arise from the same electron configuration. The quartet excited state, corresponding to state 2, arises from a different electron configuration and its minimum is offset along the two normal coordinates. The levels not interacting via spin–orbit coupling are neglected in the following calculations of absorption spectra. This approximation is not detrimental, as only the coupled states define the interference dip [2]. All other states contribute a bandshape without interference dip [5]. For the model calculations presented in the following, we use frequencies of 600 and 230 cm^{-1} for the normal

coordinates Q_1 and Q_2, respectively. These values are in the typical range of metal–ligand vibrational modes.

Two-dimensional potentials are shown in Figs. 7 and 8 to illustrate the coupling between coordinates for two different values of ΔE. In Fig. 7, ΔE is 2000 cm^{-1}, corresponding to the doublet state in Fig. 7a lower in energy than the quartet excited state in Fig. 7b. The adiabatic potential energy surface for state 1 in Fig. 7a has its minimum very close to the origin of the Q_1, Q_2 coordinate system, similar to the diabatic harmonic potential. This implies that the forbidden transition to state 1 is not expected to show long vibronic progressions, corresponding to the well known doublet bands for chromium(III) complexes where the predominant intensity is observed in origins. State 2 in Fig. 7 shows a stronger coupling between coordinates and its potential surface is tilted counterclockwise. A resolved spectrum for a transition to this state can be expected to show long progressions and unusual vibronic structure, such as the non-replica patterns discussed in Section 2, as a consequence of coupling between coordinates. Fig. 8 shows the adiabatic potentials for a ΔE value of -2000 cm^{-1}, corresponding to a higher energy for the potential minimum of state 1, the doublet state of a chromium(III) complex. In this case, both potentials show significant deformations due to coupled coordinates and they 'rotate' in opposite directions. Resolved vibronic spectra for this situation can be expected to lead to new quantitative insight on coupling between coordinates, but to the best of our knowledge, no analysis of this type has been reported for a transition metal compound.

Absorption spectra for transitions to this set of coupled potential energy surfaces are again calculated using the parameter values in Table 1 and time dependent theory [1,2,37,38], the unified approach for the calculations of all spectra in this overview. The numerical method used to calculate the autocorrelation function has been described in detail previously [51]. Instead of using pairs of two-dimensional grids to describe the potentials and time-dependent wavefunctions in coordinate space, we use a Chebyshev expansion method introduced by Kosloff and Tal-Ezer [52,53]. The wavefunction is defined by a one-dimensional set of coefficients for an optimized set of typically less than 30 basis functions, leading to a much more efficient propagation.

It is important to emphasize that the calculations in this section are not based on the adiabatic approximation, but the adiabatic surfaces in Figs. 7 and 8 are useful to illustrate the coupled coordinates and the fundamental differences between one- and two-mode models. The spin-allowed Franck–Condon transition occurs at the origin of the Q_1, Q_2 coordinate system and corresponds to the vertical arrow in Fig. 1b, ending on the harmonic surface of excited state 2. The potential

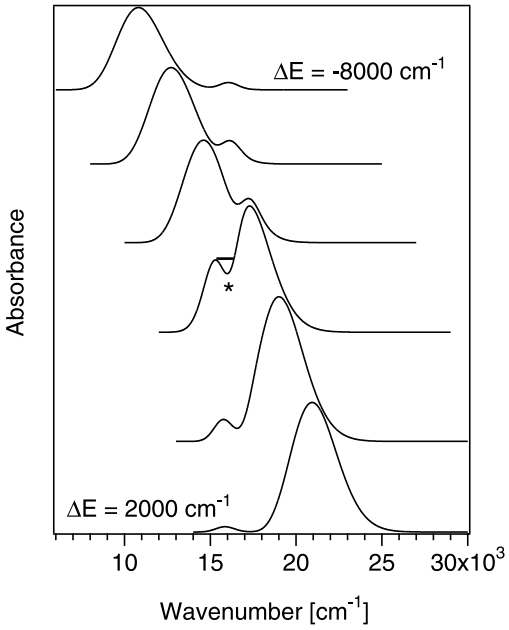

Fig. 9. Absorption spectra with interference dips calculated from the two-dimensional potential energy surfaces defined by the parameters in Table 1. Spectra are offset along the ordinate for clarity and the energy difference ΔE between excited states 1 and 2 increases from top to bottom through the list of values given in Table 1. The interference dip is marked by an asterisk in the spectrum calculated for $\Delta E = -2000$ cm^{-1}.

wells along the high-frequency coordinate are steep, resulting in a broad overall absorption band. The shallow cross section along the low-frequency coordinate Q_2 leads to a narrow overall absorption band. The interference dip in the spectrum is a consequence of the coupling between the excited states 1 and 2, which leads to coupling between coordinates, an effect easily seen from the adiabatic potentials in Figs. 7 and 8. The two-dimensional surfaces combine the effects of the low- and high-frequency modes with the electronic mixing for each point of the surfaces. This analysis of the two-dimensional surfaces illustrates the factors influencing the shape of an interference dip as shown in the calculated absorption spectra of Fig. 9. If only one normal coordinate is involved, the width of the interference dip is larger by a factor of two than the vibrational frequency [2], as shown by the experimental and calculated spectra of $Ni(H_2O)_6^{2+}$ in Fig. 6. The narrowest interference dip calculated from coupled two-dimensional potentials in Fig. 9 is on the order of 950 cm^{-1}, a value in between the doubled frequencies of the two normal modes. The lower-frequency mode is therefore important in defining the shape of the interference dip, even if the overall band envelope is determined by the higher-frequency mode. This is illustrated for $Cr_2F_9^{3-}$ in Fig. 6, where a low-frequency mode leads to the exceptionally narrow interference dip [26]. It is important to emphasize again that the calculations in Fig. 9 are not restricted to the adiabatic surfaces and an

essential factor leading to interference dips is the wavepacket amplitude transfer between the two surfaces [1,2,4,5]. The interference dips shown in Figs. 6 and 9 show that coupling between normal coordinates cannot be neglected for the analysis of electronic spectra, even if no vibronic structure is resolved.

4. Summary and conclusions

The simple potential energy surfaces defined by Eq. (1) can be used to explore spectroscopic manifestations of coupling between normal coordinates. The origin of the coupling term for these model cases is straightforward and depends on vibrational frequencies and non-zero offsets of potential minima along the normal coordinates. This model illustrates the importance of coupled normal coordinates in transition metal compounds with resolved vibronic spectra that show non-replica patterns and in unresolved spectra with interference dips. The combination of calculated and experimental spectra provides insight on coupled modes. Spectra with resolved structure are needed to further explore these effects.

Acknowledgements

We thank Dr Myriam Triest, Benoit Cromp, Professor Tucker Carrington (Université de Montréal), John K. Grey, Professor I.S. Butler (McGill University), Dr Ralph Schenker, Professor Hans U. Güdel (Universität Bern) and Professor Jeffrey I. Zink (University of California, Los Angeles) for collaborations and helpful discussions. Financial support from the Natural Sciences and Engineering Research Council (Canada) is gratefully acknowledged.

References

[1] C. Reber, J.I. Zink, Comments Inorg. Chem. 13 (1992) 177.
[2] C. Reber, J.I. Zink, J. Chem. Phys. 96 (1992) 2681.
[3] D. Wexler, J.I. Zink, Inorg. Chem. 34 (1995) 1500.
[4] D. Wexler, J.I. Zink, C. Reber, J. Phys. Chem. 96 (1992) 8757.
[5] G. Bussière, C. Reber, J. Am. Chem. Soc. 120 (1998) 6306.
[6] J.K. Grey, M. Triest, I.S. Butler, C. Reber, J. Phys. Chem. Sect. A 105 (2001) 6269.
[7] K.L. Bray, Top. Curr. Chem. 213 (2001) 1.
[8] G. Bussière, R. Beaulac, B. Cardinal-David, C. Reber, Coord. Chem. Rev. 219–221 (2001) 509.
[9] T. Fuji, T. Saito, T. Kobayashi, Chem. Phys. Lett. 332 (2001) 324.
[10] M. Ceotto, F.A. Gianturco, J. Phys. Chem. Sect. A 105 (2001) 5197.
[11] G.M. Sando, K.G. Spears, J.T. Hupp, P. Thusgaard Ruhoff, J. Phys. Chem. Sect. A 105 (2001) 5317.
[12] G.M. Sando, K.G. Spears, J. Phys. Chem. Sect. A 105 (2001) 5326.
[13] D.J. Tannor, J. Chem. Phys. 91 (1989) 2324.
[14] L.J. Butler, Annu. Rev. Phys. Chem. 49 (1998) 125.
[15] D.J. Tannor, J. Phys. Chem. 92 (1988) 3341.
[16] D. Wexler, J.I. Zink, J. Phys. Chem. 97 (1993) 4903.
[17] D.S. Talaga, J.I. Zink, J. Phys. Chem. Sect. A 105 (2001) 10511.
[18] M.J. Riley, Top. Curr. Chem. 214 (2001) 57.
[19] K.D. Demadis, C.M. Hartshorn, T.J. Meyer, Chem. Rev. 101 (2001) 2655.
[20] J.R. Winkler, H.B. Gray, J. Am. Chem. Soc. 105 (1983) 1373.
[21] J.R. Winkler, H.B. Gray, Inorg. Chem. 24 (1985) 346.
[22] C. Savoie, C. Reber, S. Bélanger, A.L. Beauchamp, Inorg. Chem. 34 (1995) 3851.
[23] C. Savoie, C. Reber, Coord. Chem. Rev. 171 (1998) 387.
[24] C. Savoie, C. Reber, J. Am. Chem. Soc. 122 (2000) 844.
[25] U. Oetliker, C. Savoie, S. Stanislas, C. Reber, F. Connac, A.L. Beauchamp, F. Loiseau, M. Dartiguenave, Chem. Commun. (1998) 657.
[26] R. Schenker, M. Triest, C. Reber, H.U. Güdel, Inorg. Chem. 40 (2001) 5787.
[27] R.G. McDonald, R. Stranger, M.A. Hitchman, P.W. Smith, Chem. Phys. 154 (1991) 179.
[28] M.D. Sturge, H.J. Guggenheim, M.H.L. Pryce, Phys. Rev. B 2 (1970) 2459.
[29] V.R. Bermudez, D.S. McClure, J. Phys. Chem. Solids 40 (1979) 129.
[30] A. Lempicki, L. Andrews, S.J. Nettel, B.C. McCollum, E.I. Solomon, Phys. Rev. Lett. 44 (1980) 1234.
[31] M. Voda, J. Garcia-Solé, I. Vergara, A. Kaminskii, B. Mill, A. Butashin, Phys. Rev. B 49 (1994) 3755.
[32] U.R. Rodrìguez-Mendoza, V.D. Rodrìguez, V. Lavin, I.R. Martin, P. Nuñez, Spectrochim. Acta Part A 55 (1999) 1319.
[33] D. Neuhauser, T.-J. Park, J.I. Zink, Phys. Rev. Lett. 85 (2000) 5304.
[34] A. Struess, W. Preetz, Z. Naturforsch. 53b (1998) 823.
[35] F. Duschinsky, Acta Physicochim. URSS 7 (1937) 551.
[36] D. Wexler, J.I. Zink, C. Reber, Top. Curr. Chem. 171 (1994) 173.
[37] E.J. Heller, Acc. Chem. Res. 14 (1981) 368.
[38] J.I. Zink, K.-S. Kim Shin, in: D.H. Volman, G.S. Hammond, D.C. Neckers (Eds.), Adv. Photochem., vol. 16, John Wiley, New York, 1991, p. 119.
[39] J. Alvarellos, H. Metiu, J. Chem. Phys. 88 (1988) 4957.
[40] X.-P. Jiang, R. Heather, H. Metiu, J. Chem. Phys. 90 (1989) 2555.
[41] M.D. Feit, J.A. Fleck, Jr., A. Steiger, J. Comp. Phys. 47 (1982) 412.
[42] M. Triest, S. Masson, J.K. Grey, C. Reber, Phys. Chem. Commun. (2000) article 12.
[43] M.J. Frisch, G.W. Trucks, H.B. Schlegel, G.E. Scuseria, M.A. Robb, J.R. Cheeseman, V.G. Zakrzewski, J.A. Montgomery Jr., R.E. Stratmann, J.C. Burant, S. Dapprich, J.M. Millam, A.D. Daniels, K.N. Kudin, M.C. Strain, O. Farkas, J. Tomasi, V. Barone, B. Mennucci, M. Cossi, C. Adamo, J. Jaramillo, R. Cammi, C. Pomelli, J. Ochterski, G.A. Petersson, P.Y. Ayala, K. Morokuma, D.K. Malick, A.D. Rabuck, K. Raghavachari, J.B. Foresman, J.V. Ortiz, Q. Cui, A.G. Baboul, S. Clifford, J. Cioslowski, B.B. Stefanov, G. Liu, A. Liashenko, P. Piskorz, I. Komaromi, R. Gomperts, R.L. Martin, D.J. Fox, T. Keith, M.A. Al-Laham, C.Y. Peng, A. Nanayakkara, M. Challacombe, P.M.W. Gill, B. Johnson, W. Chen, M.W. Wong, J.L. Andres, C. Gonzalez, M. Head-Gordon, E.S. Replogle, J.A. Pople, GAUSSIAN-01, Gaussian, Inc., 2001.
[44] (a) J.P. Perdew, K. Burke, M. Ernzerhof, Phys. Rev. Lett. 77 (1996) 3865;
(b) J.P. Perdew, K. Burke, M. Ernzerhof, Phys. Rev. Lett. 78 (1997) 1396 (E).
[45] J.P. Perdew, M. Ernzerhof, K. Burke, J. Chem. Phys. 105 (1996) 9982.
[46] M. Ernzerhof, G.E. Scuseria, J. Chem. Phys. 110 (1999) 5029.
[47] C.J.L. Lock, G. Turner, Acta Crystallogr. Sect. B B34 (1978) 923.
[48] A. Neuhaus, A. Veldkamp, G. Frenking, Inorg. Chem. 33 (1994) 5278.

[49] V.M. Miskowski, H.B. Gray, M.D. Hopkins, in: C.-M. Che, V.W.-W. Yam (Eds.), Adv. in Trans. Met. Coord. Chem, vol. 1, JAI Press, Greenwich, CT, 1996, p. 159.
[50] M. Triest, G. Bussière, H. Bèlisle, C. Reber, J. Chem. Ed. 77 (2000) 670.
[51] B. Cromp, M. Triest, T. Carrington, Jr., C. Reber, Spectrochim. Acta Part A 55 (1999) 575.
[52] R. Kosloff, J. Phys. Chem. 92 (1988) 2087.
[53] H. Tal-Ezer, R. Kosloff, J. Chem. Phys. 81 (1994) 3967.